Contrib Mineral Petrol (2009) 157:339–358
DOI 10.1007/s00410-008-0338-5

ORIGINAL PAPER

The effect of dissolved magnesium on creep of calcite II: transition from diffusion creep to dislocation creep

Lili Xu · Jörg Renner · Marco Herwegh · Brian Evans

Received: 18 October 2007 / Accepted: 15 August 2008 / Published online: 7 September 2008

Abstract We extended a previous study on the influence of Mg solute impurity on diffusion creep in calcite to include deformation under a broader range of stress conditions and over a wider range of Mg contents. Synthetic marbles were produced by hot isostatic pressing (HIP) mixtures of calcite and dolomite powders for different intervals (2–30 h) at 850°C and 300 MPa confining pressure. The HIP treatment resulted in high-magnesian calcite aggregates with Mg content ranging from 0.5 to 17 mol%. Both back-scattered electron images and chemical analysis suggested that the dolomite phase was completely dissolved, and that Mg distribution was homogeneous throughout the samples at the scale of about two micrometers. The grain size after HIP varied from 8 to 31 μm, increased with time at temperature, and decreased with increasing Mg content (>3.0 mol%). Grain size and time were consistent with a normal grain growth equation, with exponents from 2.4 to 4.7, for samples containing 0.5–17.0 mol% Mg, respectively. We deformed samples after HIP at the same confining pressure with differential stresses between 20 and 200 MPa using either constant strain rate or stepping intervals of loading at constant stresses in a Paterson gas-medium deformation apparatus. The deformation tests took place at between 700 and 800°C and at strain rates between 10^{-6} and 10^{-3} s^{-1}. After deformation to strains of about 25%, a bimodal distribution of large protoblasts and small recrystallized neoblasts coexisted in some samples loaded at higher stresses. The deformation data indicated a transition in mechanism from diffusion creep to dislocation creep. At stresses below 40 MPa, the strength was directly proportional to grain size and decreased with increasing Mg content due to the reductions in grain size. At about 40 MPa, the sensitivity of log strain rate to log stress, (n), became greater than 1 and eventually exceeded 3 for stresses above 80 MPa. At a given strain rate and temperature, the stress at which that transition occurred was larger for samples with higher Mg content and smaller grain size. At given strain rates, constant temperature, and fixed grain size, the strength of calcite in the dislocation creep regime increased with solute content, while the strength in the diffusion creep regime was independent of Mg content. The results suggest that chemical composition will be an important element to consider when solid substitution can occur during natural deformation.

Keywords Rheology · Carbonates · Constitutive laws · Solute strengthening · Normal grain growth

Communicated by J. Blundy.

L. Xu (✉) · B. Evans
Department of Earth, Atmospheric, and Planetary Sciences, Massachusetts Institute of Technology, 77 Mass. Avenue, Cambridge, MA 02139, USA
e-mail: lilixu@mit.edu

J. Renner
Ruhr-University Bochum, 44780 Bochum, Germany
e-mail: renner@geophysik.ruhr-uni-bochum.de

M. Herwegh
Institute for Geology, University Bern, 3012 Bern, Switzerland
e-mail: herwegh@geo.unibe.ch

Introduction

In many orogenic belts, carbonate formations accumulate large strains along localized shear zones that involve

deformation by non-cataclastic processes (Bestmann et al. 2000; Burkhard 1990, 1993; Busch and Vanderpluijm 1995; Carter 1992; Heitzmann 1987; Herwegh and Kunze 2002; Molli et al. 2000; Molli and Heilbronner 1999; Pfiffner 1982; Schenk et al. 2005; Vanderpluijm 1991; Yin 1996). Owing to the extreme localization, the deformation of these marble sequences must play a key role in the overall energy budget of orogenic events.

Despite extensive field and laboratory investigations (Covey-Crump 1998, 2001; de Bresser and Spiers 1993; de Bresser et al. 2001; Goetze and Kohlstedt 1977; Griggs and Miller 1951; Heard 1963; Heard and Raleigh 1972; Renner et al. 2002; Rutter 1972, 1999; Spiers 1979; Walker et al. 1990), many questions remain concerning the exact rheology appropriate to describe natural deformation of carbonates (de Bresser et al. 2002). Various studies have focused on mechanical behavior at large strains (Barnhoorn et al. 2004; Pieri et al. 2001; Rybacki et al. 2003), the influence of porosity and pore fluids on deformation (de Bresser et al. 2005; Heard 1960; Rutter 1972, 1984; Siddiqi et al. 1997; Xiao and Evans 2003; Zhu et al. 1999), and the effect of solid second phases on strength (Bruhn et al. 1999; Dresen et al. 1998; Jordan 1987; Olgaard and Evans 1986; Renner et al. 2007; Rybacki et al. 2003; Walker et al. 1990).

In this study, we investigated the strength of high-magnesium calcite of varying Mg contents. We preformed deformation experiments using both creep and constant displacement rate loading at temperatures between 700 and 800°C, in a conventional triaxial machine at a confining pressure of 300 MPa and at strain rates between 10^{-6} and 10^{-3} s^{-1}. The conditions of these experiments are similar to those previously reported by Herwegh et al. (2003), but the current data were collected over an increased range of differential stresses—up to 200 MPa and over a slightly wider range of chemical compositions. About 80 creep experiments were performed on 17 different synthetic calcite samples with Mg contents ranging from 0.5 to 17.0 mol%. Previous work suggested that deformation under these conditions of stress, temperature, and pressure occurs by a combination of diffusion creep and dislocation creep (Herwegh et al. 2003; Walker et al. 1990). The contribution to deformation by dislocation motion becomes much larger as the differential load increases. We do not attempt to provide a complete rheological description of deformation by all dislocation mechanisms (see discussion by Davis et al. 2005; de Bresser 2002; Renner and Evans 2002), but instead we focus on the relative effect of the impurity content on strength during dislocation deformation and on the conditions at which the transition between diffusion creep and dislocation creep occurs. In order to separate the contributions of diffusion and dislocation creep mechanisms, a composite flow law was fit to the data using a non-linear inversion technique. We also performed additional grain-growth experiments under hydrostatic loading to investigate further the effect of solute impurities on growth kinetics.

Solid solutes and physical properties

Minerals often contain impurities that substitute in varying amounts for the usual ion expected from the chemical formula (Nesse 2000; Wenk and Bulakh 2004). In such cases, the impurity ions are solutes, dissolved into the crystal lattice, and when the impurities take the place of one of the stoichiometric ions, the mineral can be regarded as a substitutional solid solution. For example, natural carbonates often contain varying amounts of divalent impurity cations, for example, Fe, Mg, Mn, and Sr, which substitute for Ca (Essene 1983; Mackenzie et al. 1983). The physical properties of ceramics and semiconductors, including grain-boundary mobility, diffusion coefficients, electrical conductivity, and strength are known to be very strongly affected by solid solutes (e.g., Chiang et al. 1997; Lücke and Stüwe 1971), and similar effects may be evident in mineral solid solutions (Bai et al. 1995; Hiraga et al. 2007; Hitchings et al. 1989; Hobbs 1984; Kohlstedt 2006). For example, the solution of Fe in forsterite increases the creep rate under anhydrous conditions by factors of as much as 1,400 times (Zhao et al. 2008).

Some studies intimate that the physical properties of carbonates will also be strongly affected by solid solutes. Natural carbonate rocks tested in the laboratory are often stronger than synthetic ones, which likely contain fewer impurities (Heard and Raleigh 1972; Renner et al. 2002; Rutter 1974; Schmid 1977; Schmid et al. 1980; Walker et al. 1990). Freund and co-workers (Freund et al. 2001; 2004; Wang et al. 1996) have suggested that trace amounts of dissolved Mn (10–670 ppm) decrease the strength of calcite during both dislocation and diffusion creep, although the effect in the former regime may be small. Larger amounts of dissolved Mg do not directly affect the flow strength of the calcite aggregates in the diffusion creep regime (Herwegh et al. 2003), but, in those experiments, high Mg content correlated with smaller grain size, and this, in turn, is expected to reduce the aggregate strength during Coble creep. Mn and Mg solutes also have opposite effects on normal grain growth of calcite. The addition of Mn (less than 670 ppm) increases growth rates (Freund et al. 2001), but the addition of Mg (>7 mol%) decreases boundary mobility (Herwegh et al. 2003).

Rheological descriptions of diffusion and dislocation creep

Here we are interested in the effect of solute impurities on the creep behavior of calcium carbonate rocks. For deformation by non-cataclastic (crystal–plastic) processes, forward predictions of the strength of naturally deformed rocks can be made using constitutive laws calibrated by laboratory experiments, provided that appropriate thermodynamic conditions are simulated and controlled, and that the deformation mechanisms that operate in the experiments are also relevant to the geological processes (Kohlstedt et al. 1995; Paterson 1976, 2001; Ranalli and Murphy 1987). For a general framework of constitutive laws, see Frost (1982). The deformation mechanisms involved are probably, in general, sensitive to strain rate and temperature and have variously been termed crystal plasticity; ductile, viscous, plastic deformation; or creep. To emphasize the effect of prolonged loading, we use the generic term, creep deformation, to refer to all rate-dependent deformation occurring by motion of any crystal defect.

Three classes of equations are commonly used to represent steady-state creep of rocks. At high temperatures, small grain sizes, and/or low stresses, rocks may deform by diffusion creep:

$$\dot{\varepsilon}_{\text{diff}} = \dot{\varepsilon}_{\text{diffo}} \frac{\sigma^r}{d^s} \exp\left(-\frac{Q_{\text{diff}}}{\text{RT}}\right) \tag{1}$$

where r is usually nearly equal to 1, s may be 1–3, Q_{diff} is the activation enthalpy for self-diffusion of the slowest constituent of the mineral along the fastest available path, and $\dot{\varepsilon}_{\text{diffo}}$ is a factor that may be weakly dependent on temperature or more strongly dependent on details of the point defect chemistry.

As temperatures decrease, or grain size and stresses increase, the creep deformation will be dominated by dislocation motion. The most common constitutive equation used to describe dislocation creep in rocks at elevated temperature and slow strain rates is the power-law equation:

$$\dot{\varepsilon}_{\text{pwr}} = \dot{\varepsilon}_{\text{pwro}} \sigma^n \exp\left(-\frac{Q_{\text{pwr}}}{\text{RT}}\right) \tag{2}$$

where $\dot{\varepsilon}_{\text{pwro}}$ is a pre-exponential factor, perhaps containing a dependence on chemical fugacity; σ is the differential stress; n is the stress exponent of strain rate; RT is the standard Boltzmann term, with gas constant, R, and absolute temperature, T; Q_{pwr} is the activation enthalpy for creep.

At low-temperatures, high stresses or fast strain rates (as defined by Frost 1982), creep deformation may be limited either by cross-slip (de Bresser and Spiers 1993) or dislocation glide (Renner and Evans 2002). The latter authors used an empirical equation for the power-law breakdown region of the form:

$$\dot{\varepsilon}_{\text{plb}} = A_{\text{plb}} \sigma^2 \exp\left(\frac{\sigma}{\sigma_p}\right) \exp\left(-\frac{Q_{\text{plb}}}{\text{RT}}\right) \tag{3}$$

where A_{plb} is a material constant, Q_{plb} is the activation energy for dislocation creep, and $\sigma_p = \left(\sum_{p,0} + Kd^{-m_p}\right)(T_m - T)$ is the resistance to glide, which is composed of an intrinsic Peierls stress and a grain-size dependent back stress. T_m denotes the melting temperature (Renner et al. 2002). Several other formulations for stress-activated deformation might also be used (Renner and Evans 2002), and we do not regard this formulation as definitive. In this study, we use (3) as an empirical fit to data in the dislocation creep regime, but suggest caution in using this creep law to extrapolate to natural conditions.

In the discussion below we identify these regimes as diffusion creep, high-temperature dislocation creep, and low-temperature dislocation creep, respectively. The low-temperature creep equation is sometimes called plastic, but, in fact, all three equations can be said to be creep equations because they each predict a non-zero inelastic strain rate under prolonged load. Some caution in using the equations is appropriate, however. Diffusion creep of carbonates at high temperatures seems to be described well by Eq. (1), but the high-temperature dislocation creep equation (2) does not accurately represent the mechanical behavior over a significant range of conditions (see reviews by de Bresser 2002; Walker et al. 1990). For example, n values found by fitting data to (2) are usually between 3 and 9, but these values increase with increasing stress and are not constant even over small intervals in stress. Eq. (3) is successful in fitting most of the experimental data for several calcite rocks, but it is largely empirical. In fact, none of the current constitutive models are capable of adequately explaining all the details of the mechanical behavior for dislocation creep of carbonate rocks. Further work is needed to formulate a set of robust constitutive equations, which are firmly based on observable microstructure variables and fundamental microphysics. Because of this uncertainty, in the following discussion, we may often simply refer to deformation by dislocation motion, as dislocation creep, without making a distinction between high and low temperature regimes.

Methodology of experiments

Sample preparation and apparatus

Samples were prepared from mixtures of reagent-grade calcite powder (5 μm grain size, Mallinckrodt Inc.) and

ground natural dolomite powder (Microdol Super from Alberto Luisoni Mineralstoffe; 2 μm grain sizes). The hot isostatic pressing (HIP) technique was described in detail previously (Herwegh et al. 2003; Renner et al. 2002). Powders were mixed in proportions to produce marbles with magnesium solute contents (after HIP) of 0.5, 3.0 to 17.0 mol% (Fig. 1). The different Mg-calcites will be referred to as Mgcc, −20, −40,…,−80, where the numbers indicate the temperature at which the solid-solution is at saturation (e.g., Mgcc-20 has 0.5 mol% Mg dissolved in the calcite lattice; calcite with that composition is saturated with Mg at 200°C). After mixing, powders were dried in an oven at 110°C and cold-pressed into thin-walled (0.3 mm) iron shells using a uniaxial stress of about 100 MPa. The cold-pressed aggregates, whose initial porosity was about 25%, were dried overnight and then loaded into an iron jacket along with Al_2O_3 and ZrO_2 pistons (Fig. 2).

HIP

To fabricate the synthetic marbles, the sample assembly was pressurized to about 225 MPa and then heated to 850°C at a rate of 15°C/min in an internally heated Paterson apparatus (Paterson 1990). The HIP step lasted from 2 to 30 h at 850°C and 300 MPa confining pressure. To monitor densification, we applied an axial stress of less than 3 MPa (<0.2 KN) and measured changes in sample length during heat-up, pressurization, and the isothermal HIP. The temperature was monitored by three Pt-Pt/Rh thermocouples inserted in the furnace and by an additional chromel-alumel thermocouple reaching the top of the sample through a bore in the ceramic pistons. The temperature at the top of the sample varied by less than ±5°C throughout the experiments. Before the experiments, we calibrated the furnace to guarantee a flat thermal profile along the sample (spatial temperature variations are estimated to be <±2°C).

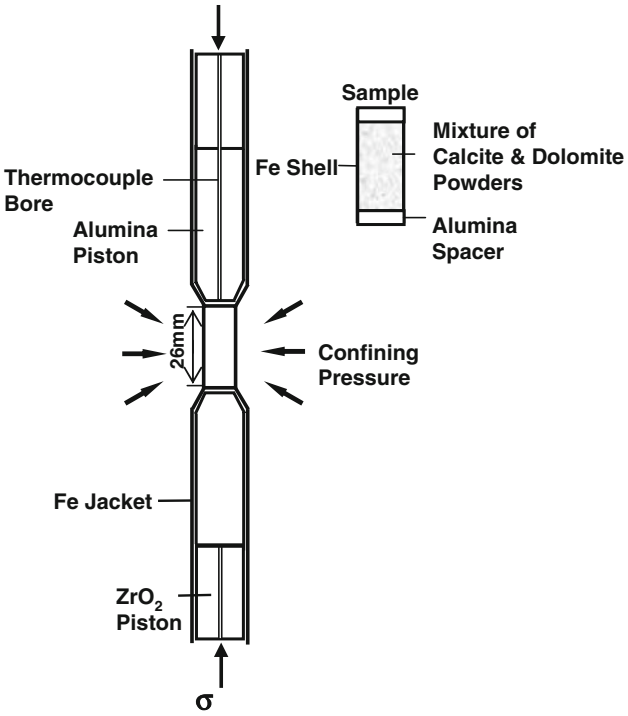

Fig. 2 Schematic cross-section of the sample assembly for the grain growth and deformation experiments. See Renner et al. (2002) for a complete description of the apparatus and of the accuracy of the measurements

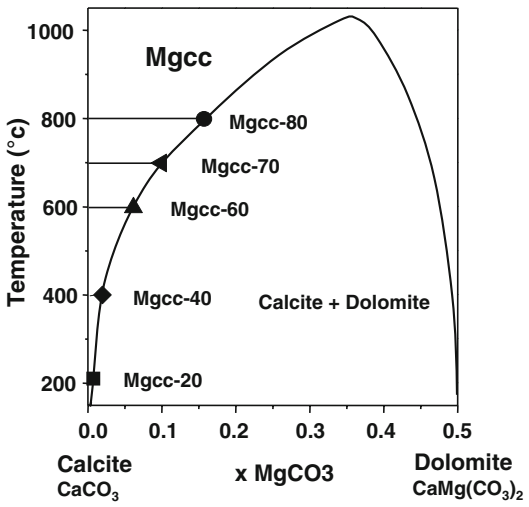

Fig. 1 Calcite–dolomite solid-solution system; after Anovitz and Essene (1987). *Symbols* indicate the molar concentration of Mg in calcite for the various samples and the temperature at which each composition would saturated in Mg. The labeling is the same as in Herwegh et al. (2003). Two new composition Mgcc-20 and Mgcc-40 have been added in this study. All samples were produced using HIP at 850°C; all solid solutions used in this study should be stable for deformation at 800°C. The most-concentrated solid solutions (Mgcc-80) may have undergone exsolution during deformation at 700–800°C; but the remainder should have been stable at all conditions

During the initial portion of the HIP, Mg-calcite is formed from the mixture of calcite and dolomite powders by a complex combination of densification, grain-boundary diffusion, volume diffusion, and chemically induced grain-boundary migration (see Herwegh et al. 2003). During this short transition period, a dense compact aggregate of high-magnesian calcite is formed with an average grain size that is smaller than the original powder sizes. Additional heat-treatment under isostatic stress (longer HIP time) resulted in normal grain growth. By interrupting the HIP process at very short times, we ascertained that normal grain growth was underway after 1,000 s and that the average grain size of the aggregate was about 5 μm. Ten additional HIP experiments of durations up to 18 h were conducted to investigate normal grain growth rates.

Chemical analyses of the mixtures after HIP treatments were done in electron microprobe (JEOL JXA-733) with spatial resolution of ~ 2 μm through X-ray emission spectrometry. At the scale of the probe dimensions, (~ 2 μm), the aggregates were spatially homogeneous. The microprobe results provide quantitative checks on the Mg content of the synthetic marbles. The microprobe measurements also indicate the presence of trace impurities of Fe, Mn, and Sr. These three cations are present in amounts much less than 0.1%; i.e., concentrations that are too small to be measured very accurately in the microprobe. Because these impurities are probably contained within the natural dolomite powder, their concentrations in the aggregates are likely to co-vary with the Mg content.

Deformation tests

We performed deformation tests on other samples immediately after the HIP step by reducing the temperature at 15°C/min to the run temperature (800, 750, or 700°C) and then allowing the thermal profile to equilibrate for about 20 min. The confining pressure was adjusted to 300 MPa, if necessary, and maintained at that value throughout the experiment. Displacement of the axial loading piston is quantified using a linear variable differential transformer (LVDT), which can detect a minimum displacement increment of 0.3 μm, i.e., a minimum detectable strain increment of 1.5×10^{-5}. The load is measured internally with uncertainty of 20 N (i.e., about 0.3 MPa in axial stress). The strength of the metal shell (iron) at the experimental conditions was taken into account using a correction procedure from Renner et al. (2002); more details of the apparatus can also be found there.

Deformation tests were done either with constant strain rate or constant stress (Table 1). Strain rates varied from $\sim 10^{-6}$ to 10^{-3} s^{-1}; and the total inelastic strain of the sample was about 20% or less for most tests. When subsequent examination indicated that the sample had barreled, the mechanical data were discarded to prevent artifacts induced by inhomogeneous deformation. The duration of a deformation test was usually less than 1 h. After deformation, samples were unloaded first and quenched immediately after unloading by reducing the confining pressure and turning off the furnace simultaneously. The temperature in the sample drops from 700 to 300°C in less than one minute. Recovery experiments in heavily deformed calcite single crystals indicate that dislocation densities are reduced by less than 20% over a period of 2 h at 600°C (Liu and Evans 1997). Thus, the dislocation microstructure is probably affected very little by the quench procedure.

At the end of each hydrostatic or triaxial experiment, a polished thin section was made to measure the grain size. Micrographs were recorded from optical observations made in reflected polarized light, and a tracing of the grain boundaries in the sample was made by hand, using Imagepro software and some manual adjustment. Using the software, the area of each grain was calculated, and the grain size recorded as the diameter of a circle with equivalent area. In each sample at least 300 grains were measured. To compare with previous grain growth studies that used mean intercept length (e.g., Covey-Crump 1997; Schmid 1977; Tullis and Yund 1982), we also calculated the mean intercept length (D_{2D}) using equation $D_{2D} = \pi \overline{A}_\alpha / \overline{L}_p$ (Underwood 1970, p. 42), where $\overline{A}_\alpha$ is the mean area of grains in the 2D image and $\overline{L}_p$ is their mean perimeter length. The sample porosity after the experiment was calculated using either a geometric method, i.e., weighing a sample with known dimensions, or by calculating the area fraction of porosity from an SEM image. Dislocation structures of HIPed and deformed samples were studied using a transmission electron microscope (TEM) operating at 200 kV.

Results

Microstructures formed under hydrostatic and conventional triaxial loading

After the initial period of reaction and mixing, normal grain growth occurs. Figure 3a–c shows photomicrographs of Mgcc-20, Mgcc-60, and Mgcc-80 after HIP for 2 h at 850°C and 300 MPa. Grain boundaries are slightly curved; triple junctions have angles of approximately 120°. The grain sizes appear to be approximately in lognormal distribution (Fig. 4). The grain size after HIP increases with longer hot-pressing time and lower bulk impurity content (Mg content > 3.0 mol%, Fig. 5), consistent with earlier observations (Herwegh et al. 2003). The total porosity of samples after HIP is usually between 0.5 and 1%, and does not systematically correlate with Mg content. During deformation, both grain growth and grain refinement occur (Figs. 3d–f, 4). The magnesium content in Figs. 3d–f varies in the same order as in Figs. 3a–c. The grain sizes of different samples range from 8 to 31 μm.

We did not perform detailed quantitative analysis of the dislocation structure of these samples, but cursory inspection does not indicate an obvious variation of the dislocation morphology with variations in magnesium content. Bright field TEM micrographs of a deformed sample (Mgcc-20) show free dislocations, microtwins, and dislocation networks (Fig. 6). Free dislocations of various orientations (Fig. 6a) indicate the activation of multiple slip systems. Cell structures and sub-grain boundaries (Fig. 6b) probably indicated that recovery processes, such

Table 1 Conditions and results of the deformation experiments

Run no.	T (°C)	Stress (MPa)	Strain rate (s^{-1})	Strain (%)	Grain sizes[a]	Porosity[b]	Description
C814	794	22 creep	1.2×10^{-6}	0.8	16.0 ± 3.1	1.5% (2.4%)	Mgcc-60, HIP-2 h
		44	5.3×10^{-6}	1.7			
		65	2.1×10^{-5}	2.6			
		86	9.2×10^{-5}	4.1			
	691	93	1.0×10^{-5}	4.7			
		126	6.7×10^{-5}	8.1			
		104[d]	3.2×10^{-5}	8.9			
		77[d]	9.1×10^{-6}	8.8			
		64[d]	8.0×10^{-6}	8.5			
		39[d]	2.5×10^{-6}	8.9			
C817	Mgcc-70, HIP-2 h, load-cell signal unstable						
C818	795	15 creep	9.2×10^{-6}	1.1	6.7 ± 0.9	0.5%	Mgcc-70, HIP-2 h
		40	2.4×10^{-5}	2.5			
		82	1.1×10^{-4}	4.3			
	694	15	1.7×10^{-6}	6.8			
		38	3.7×10^{-6}	7.3			
		82	1.4×10^{-5}	8.3			
		120	4.1×10^{-5}	9.6			
		173	3.4×10^{-4}	14.1			
C819	Mgcc-80, HIP-0.5 h, jacket leak						
C820	801	19 creep	4.8×10^{-5}	2.5	7.0 ± 1.6	0.7% (2.7%)	Mgcc-80, HIP-2 h
		48	1.3×10^{-4}	4.8			
		81	3.5×10^{-4}	8.5			
		111	1.3×10^{-3}	15.7			
	697	22	1.1×10^{-5}	17.8			
		35	2.1×10^{-5}	18.5			
		59	4.3×10^{-5}	19.6			
		83	7.5×10^{-5}	20.8			
		129	2.0×10^{-4}	24.3			
C826	799	49 creep	1.0×10^{-6}	0.7	17.7 ± 3.0	(0.7%)	Mgcc-60, HIP-20 h
		66	2.1×10^{-6}	1.0			
		91	6.2×10^{-6}	1.5			
		108	1.9×10^{-5}	2.1			
		124	5.6×10^{-5}	3.1			
		140	1.7×10^{-4}	5.0			
		151[d]	3.7×10^{-4}	8.1			
		161[d]	1.3×10^{-3}	19.6			
C827	982	55 creep	2.3×10^{-6}	5.7	11.7 ± 1.7	0.5% (4.9%)	Mgcc-60, HIP-2 h
		125	1.5×10^{-4}	10.1			
		139[d]	9.1×10^{-4}	33.3			
C855	Mgcc-60, HIP-20 min, jacket leak						
C856	695	86	7.6×10^{-6}	1.0	8.7 ± 1.6	(3.3%)	Mgcc-70, HIP-2 h
		108	3.6×10^{-5}	3.2			
		131	1.5×10^{-4}	7.5			
		139	4.6×10^{-4}	16.3			
		99[d]	2.2×10^{-4}	20.2			
		126[d]	7.4×10^{-4}	27.5			

Table 1 continued

Run no.	T (°C)	Stress (MPa)	Strain rate (s^{-1})	Strain (%)	Grain sizes[a]	Porosity[b]	Description
C857	801	104	5.3×10^{-4}	4.9	8.5 ± 2.0	0.5% (3.3%)	Mgcc-80, HIP-6 h, weakening
		100	1.1×10^{-3}	17.4			
		72	7.0×10^{-4}	21.9			
C859	800	67	1.2×10^{-4}	+16.8	13.1 ± 3.0	(1.8%)	Mgcc-65, HIP-2 h
		52	8.5×10^{-5}	−15.5			
		59	1.1×10^{-4}	+19.3			
		57	1.0×10^{-4}	−5.9			
C869	807	85	1.1×10^{-4}	3.8	12	0.5%	Mgcc-80, HIP-18 h
		96	2.1×10^{-4}	7.4			weakening
	756	97	1.0×10^{-4}	10.5			
	695	73	1.4×10^{-5}	12.3			
		97	2.1×10^{-5}	13.3			
	805	79	1.8×10^{-4}	16.8			
		100[d]	3.3×10^{-4}	21.9			
C870	800	76	2.4×10^{-4}	4.6	9		Mgcc-60, HIP-2 h
		85	6.3×10^{-4}	9.9			
	751	89	2.4×10^{-4}	13.0			
		98	3.5×10^{-4}	16.8			
	694	164	3.2×10^{-4}	20.8			
C880[c]	804	132	8.2×10^{-4}	5.0	7	0.5%	Mgcc-60, HIP-2 h
		115		10.0			
		101		20.0			
		90[d]		43.3[d]			
C883[c]	797	193	8.5×10^{-4}	5.0	7	0.5%	Mgcc-80, HIP-30 h
		176		10.0			
		143		20.0			
		127[d]		31.8			
C900	792	124	7.8×10^{-4}	6.6	17	0.5%	Mgcc-60, HIP-4 h
	745	159	8.1×10^{-4}	11.3			
	695	208	8.5×10^{-4}	15.8			
	743	179	9.3×10^{-4}	20.6			
C942	785	65	4.9×10^{-4}	7.0	25		Mgcc-40, HIP-2 h
		52	1.3×10^{-4}	10.8			
		38	3.9×10^{-5}	15.8			
		61	4.2×10^{-4}	21.4			
		35	4.2×10^{-5}	24.2			
C948	800	42	3.1×10^{-4}	4.4	27	3.8%	Mgcc-20, HIP-2 h
		38	1.2×10^{-4}	8.1			
		30	3.5×10^{-5}	10.8			
		46	3.4×10^{-4}	15.5			
		31	3.8×10^{-5}	18.6			
C1038[c]	800	143	8.9×10^{-4}	5.0	22	0.5%	Mgcc-60
		151		10.0			HIP-18 h
		128		14.7			

[a] Average intercept length of deformed samples

[b] Quench density calculated using the geometric method or from SEM images (in parenthesis)

[c] Constant strain rate tests, flow stresses are given at different strains

[d] Data discarded due to sample barreling or strain weakening

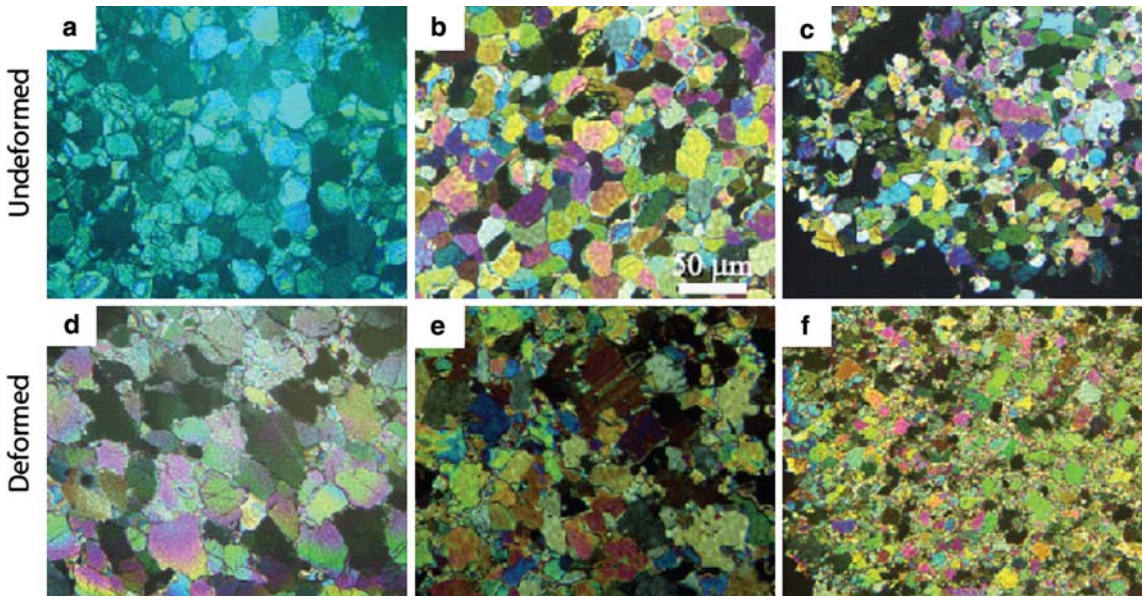

Fig. 3 Optical micrographs in cross-polarized light for undeformed (**a**–**c**) and deformed (**d**–**f**) samples with Mg concentration of 0.5 mol% (**a**, **d**), 7.0 mol% (**b**, **e**), and 17.0 mol% (**c**, **f**). All were prepared using a HIP step of 2 h. Undeformed (**a**–**c**) samples contain isometric grains with straight or gently curved boundaries. The deformed samples (**d**–**f**) shown here were deformed under multiple stress conditions, at relatively high stresses. They contain small recrystallized neoblasts, along with larger grains that have undulate boundaries. See Fig. 4 for grain size distribution analysis. *Scale bar* for all micrographs shown in (**b**). Note that the magnesium content in Fig. 3d–f (samples C948, C814, and C820) varies in the same order as in Fig. 3a–c

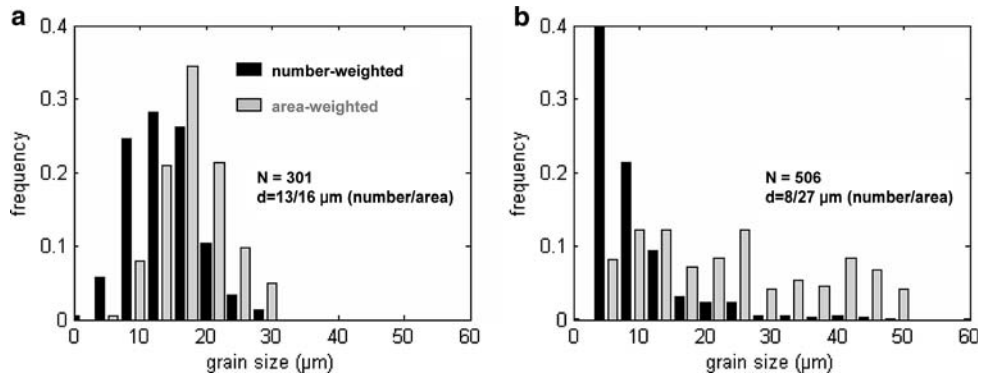

Fig. 4 Grain size distributions of samples with 7.0 mol% Mg after HIP for 2 h at 850°C (**a**) and after deformation (**b**, ~9% strain). *Black bars* and *gray bars* represent number-weighted and area-weighted grain size distributions, respectively. The average grain sizes are indicated. In each sample, at least 300 grains were measured; the grain dimension is determined by calculating the diameter of a *circle* with an area equivalent to that particular grain. Note that the deformed sample contains a large number of small grains but also a few large grains that covers a considerable area fraction

as climb, were operating. Our starting material has relatively low dislocation densities, well below 1×10^{13} m^{-2}, but those increased during deformation to greater than 2×10^{13} m^{-2}. Such densities are comparable to those in natural calcite rocks deformed in the laboratory (de Bresser 1996; Goetze and Kohlstedt 1977; Schmid et al. 1980). Microtwins (Fig. 6d, <1 μm thick) are infrequently observed; these are usually observed in natural calcite that deformed at less than 150°C (Burkhard 1993).

Creep of high-magnesium calcite

If the duration of the test is short compared to the time necessary for the grain size to evolve, then the test can be regarded as occurring at a fixed grain size. Additionally the same creep conditions can be revisited at the beginning and end of the test (as described immediately below). For samples with Mg content of 0.5–17.0 mol%, grain sizes in the range of 20 and 12 μm could be produced by varying

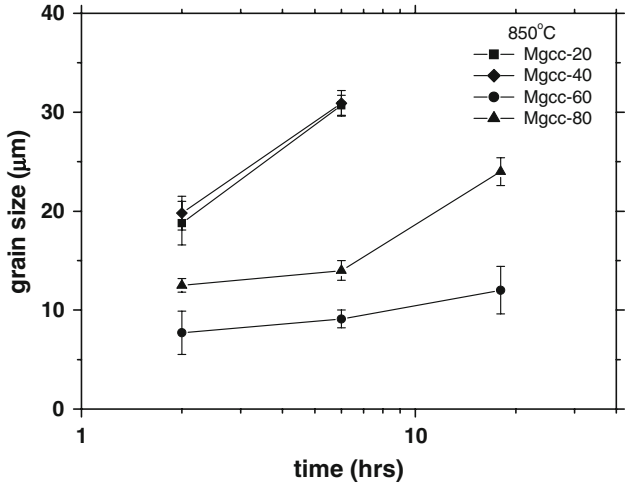

Fig. 5 Evolution of grain size for samples of different compositions as a function of the duration of the HIP step (at 850°C). All samples were loaded under isostatic stresses only and held for different times at constant temperature. Slower grain growth rates correlate with higher magnesium content

the HIP time intervals from 2 to 30 h. The strength of Mg-calcites determined from these constant strain rate tests ($\sim$3.1–8.5 $\times$ 10^{-4} s^{-1} at 800°C and 300 MPa) indicated that the strength of calcite increases with magnesium content (Fig. 7a). The strain rates are high and all these samples are deformed in dislocation creep regime.

Typical differential stress ($\sigma_1 - \sigma_3$) versus strain rate data are shown in Fig. 7b. Both the grain size and the magnesium content affect the strength. At low strain rates, the strength of Mg-calcite correlates with grain size, rather than Mg content; and n values are nearly unity (Fig. 7b), consistent with previously published results. At higher strain rates, the flow strength of calcite strongly depends on the Mg content, although the data for the high Mg-calcites show more scatter. In general, n values increase with stress, but decrease with increasing Mg content at higher stresses used in these experiments.

Magnesium solute could affect the mechanical behavior of calcite in at least three ways: first, the elastic modulus of calcite increases with increasing Mg content (Zhang and Reeder 1999); second, the strength of calcite in the diffusion creep regime is indirectly affected by the suppression of grain growth (Herwegh et al. 2003); and third, Mg solutes may interact with dislocations as individual obstacles or solute clouds. The first two effects and the effect of temperature can be eliminated by normalizing the strength by the appropriate shear modulus (G) and by multiplying strain rate by $\exp(Q_{\text{diff}}/\text{RT}) \times d^s$, where Q_{diff} and s are the activation energy and grain size sensitivity factor in the diffusion creep regime (Herwegh et al. 2003) and d is the grain size.

Three distinctive regimes of mechanical behavior may be identified in Figs. 7c: First, at low stresses, $\sigma/G < \sim 10^{-3}$, the strength is directly proportional to the cube of the grain size and the stress exponent of strain rate, n, is about 1, behavior that we interpret to indicate Coble creep. The normalized strain rate, $\dot{\varepsilon}_{\text{normal}} = \dot{\varepsilon}\exp(\text{Q}_{\text{diff}}/\text{RT})d^3$, is a linear function of normalized stress, $\sigma_{\text{normal}} = (\sigma_1 - \sigma_3)/\text{G}$, and shows less scatter than the raw data because the effect of grain size has been removed. The difference in normalized strength at a fixed normalized strain rate is small and

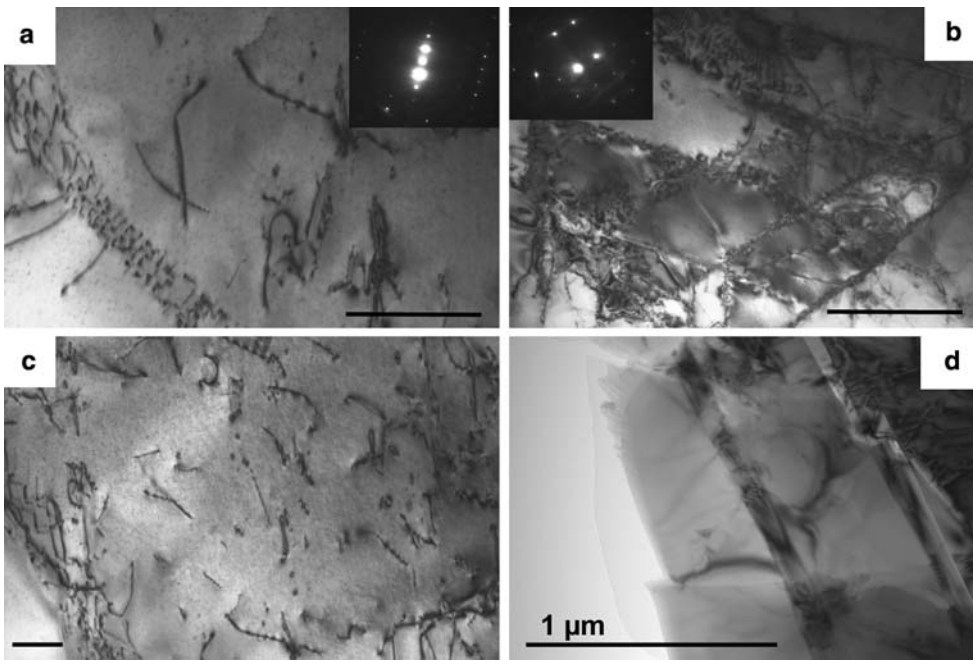

Fig. 6 Transmission electron microscope (*TEM*) micrographs of a sample (C942) deformed in dislocation creep regime. *Scale bars* in each micrograph are 1 μm. In general, the samples show widely spaced sub-grain networks (**a**–**c**) that interact with each other (**b**) and with dislocations within the interior of the subgrains. Dislocations of various orientations indicate slip on several systems. The free dislocation density is relatively low (**c**). A few microtwins (**d**), with widths of about 30–100 nm, are infrequently observed

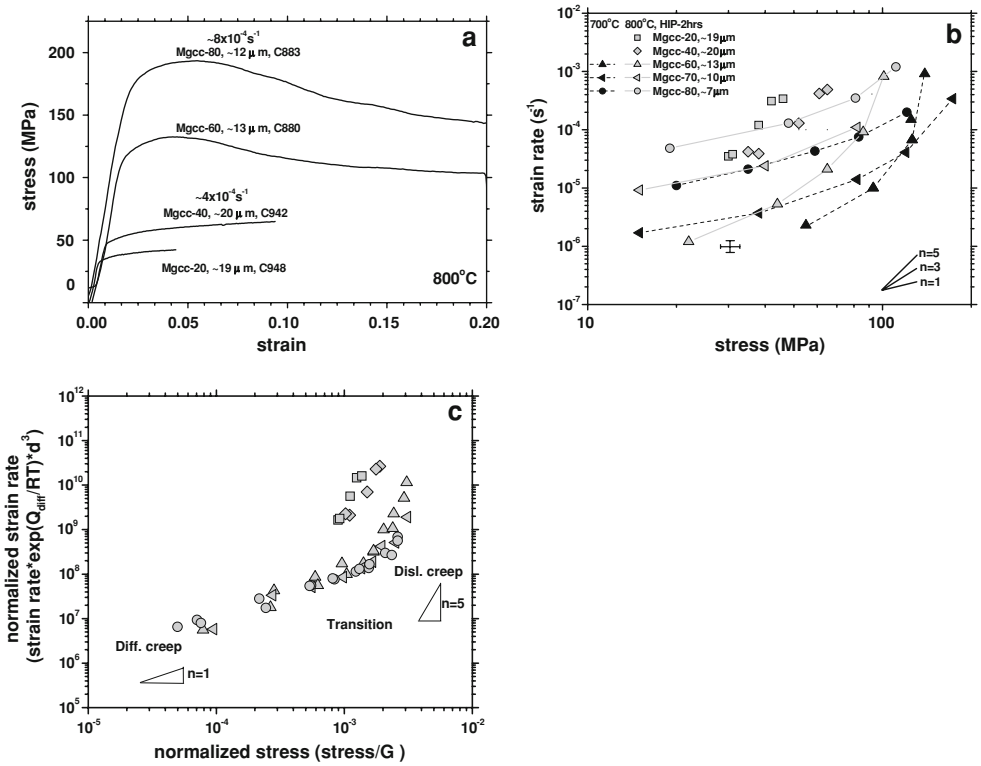

Fig. 7 **a** Constant displacement rate tests on different Mg-calcites at 800°C and 300 MPa. The strain rates are high and all these samples deformed in dislocation creep regime. Strain weakening is obvious in some of the tests at high differential stress (>100 MPa). Grain sizes at the starting of the deformation are estimated from the grain growth data and shown as indicated. **b** Mechanical data from stress-stepping and creep tests after HIP for 2 h at 850°C and deformation at 800°C (*gray symbols*) and 700°C (*black symbols*). The *crossed error bars* represent the absolute uncertainty of the data points. The data are scattered because both grain size and Mg content varies. There are, however, systematic trends. Notice that the stress sensitivity of strain rate (n) increases with differential stress, and that the transition from diffusion creep to dislocation creep (identified by the change in slope) is shifted to higher stress for samples with higher Mg content (i.e., 700°C). **c** Normalized strain rate versus normalized stress. When the differential stress is normalized by the shear modulus adjusted to reflect changes in the elastic modulus owing to different compositions, and strain rate is normalized by grain size and a kinetic term appropriate for diffusion creeps, much of the scatter seen in (**b**) is removed. The normalization of the strain rate removes the effect of grain size which is systematically smaller in the high Mg calcites. Notice that the low Mg-calcite aggregates are weaker in the dislocation creep region. The strength of calcite increases with Mg content in dislocation creep regime, but not in the diffusion creep regime

does not vary systematically with Mg content. Second, at intermediate stresses (normalized stress $\sim 10^{-3} - 2 \times 10^{-3}$), n varies from about 1 to greater than 3, a region we interpret as transitional between diffusion creep and dislocation creep. Third, at high stresses (normalized strength $> 2 \times 10^{-3}$), n is greater than 3; the normalized strengths vary directly with Mg content; and we suppose that deformation occurs by dislocation creep. At a fixed temperature and strain rate, the transition between the region of linear stress/strain rate behavior and the highly non-linear region occurs at higher stresses and larger grain sizes for calcite with higher Mg concentration (Fig. 11).

To study the effect of loading history (accumulated strain and elapsed time) on the strength of Mg-calcite, we revisited the initial deformation conditions on samples subjected to multiple strain rate steps. The small effect of the accumulated strain on the strength of low Mg-calcite is consistent with previous studies on pure synthetic calcite (Renner et al. 2002). By contrast, high Mg-calcite tends to exhibit increased strain rates after deformation in the intermediate- to high-stress regime (Table 1). In one test (C859), the sample was shortened in compression, extended at different conditions, and then shortened under the initial conditions. It was weaker than the unstrained sample by about 29% after the intermediate cycle in tension. In fact, most samples became weaker at low stress conditions when subjected to intermediate deformation at higher stresses (Fig. 8). Revisiting lower stresses after deformation in the intermediate- to high-stress regime affected the strength of high Mg-calcite more than that of low Mg-calcite (e.g., step 5 for sample Mgcc-70). Also, notice that there is also strain weakening in high Mg-calcites (Mgcc-60 and Mgcc-80) over a strain interval of about 20%. Optical micrographs of some of these samples, i.e.,

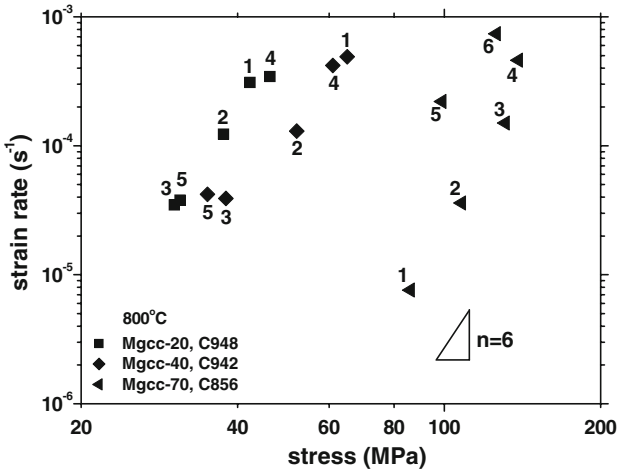

Fig. 8 Data reproducibility is shown by creep step tests. Numbers indicate the order in which the tests were conducted. The sample with the highest magnesium content indicates a strength that changed when the initial stress was revisited

deformed at higher stress levels, show many fine recrystallized grains (Fig. 3e, f).

Discussion

Both the grain-growth kinetics and the strength of calcite during dislocation creep are strongly affected by the addition of solutes from the dolomite. Interestingly, the diffusion creep strength does not seem to be affected, provided that comparisons are done at similar grain size (Herwegh et al. 2003). Within the dislocation creep regime, absolute values of strength at a given strain rate correlated directly with the Mg solute content, and, we argue below that the transition from diffusion creep to dislocation creep occurred at larger grain sizes when the Mg content was elevated. In some cases, the relation between stress and strain rate changed when lower stresses were revisited during the stress-step experiment. This result suggests an evolution of some mechanically important state variable, probably grain size. One possibility for this change is an increased contribution of diffusion creep within the population of small recrystallized grains formed during deformation at higher stresses. But, other explanations are also tenable. For example, there might be changes of the fine-scale impurity distribution. It is known that submicron-scale chemical modulations exist in dolomite and high-magnesium calcite (e.g., Wenk et al. 1983). Weakening could also occur, if, during the experiment, the dislocation structure or mobility evolved in ways that were not directly proportional to the applied stress, for example owing to release of an impurity cloud around dislocations. Further study is needed to determine the exact cause. In the remainder of this paper, we exclude any strength data that may have exhibited such changes and concentrate only on data taken during constant loading conditions, or when stresses were monotonically increased.

An additional caveat should be recognized. The dolomite used in this study comes from a natural mineral source, and contains some traces of Fe, Mn, Al, and Sr. Chemical compositions of minerals were determined by wavelength dispersive spectrometry with a JEOL JXA-733 electron microprobe. The microprobe measurements of those impurity concentrations (<0.1%) are semi-quantitative and the concentrations do not appear to vary from one aggregate to another. But, because the impurities are contained within the dolomite, it is most likely that all the impurities actually co-vary with the Mg content. Without considerable additional work, we cannot definitively implicate one or another cation as the cause of the strengthening. However, it is universally true that deformation tests indicate that all dolomites are stronger than calcites under the same conditions (Davis et al. 2005); and thus, as a first approximation, it seems the simplest interpretation to assume that Mg is indeed the source of strengthening. Still, one should remember that other ions contained within the dolomite at the trace level might have an influence on strength.

Effect of Mg on grain growth of calcite

Grain-growth rates can be influenced by many factors, including pores, fluids, solute impurities, and second phases (Atkinson 1988; Drury and Urai 1990; Evans et al. 2001; Urai et al. 1986; Yan et al. 1977). In metals and ceramics, solid solutes may either increase grain growth rates, as happens with segregation of Al to boundaries in tetragonal zirconia stabilized by yttria (Chokshi et al. 2003), or they may exert solute drag on the boundary, as occurs with the addition of magnesia to alumina (Bae and Baik 1994; also see reviews by Powers and Glaeser 1998; Rollett 2004; and Yan et al. 1977).

For calcite rocks, grain growth in Solnhofen limestone is slow compared to synthetic marbles, whether doped with Mg or not (Fig. 9a) (Evans et al. 2001; Olgaard and Evans 1988; Schmid 1977; Tullis and Yund 1982). Previous studies suggest that the reduced grain-growth rate of Solnhofen limestone can be attributed to the influence of second phases, solute impurities, and the reactions of accessory minerals. In general, synthetic marbles with added water have higher grain-growth rates than samples with the same porosity, but no added water (Covey-Crump 1997; Olgaard and Evans 1988). Samples with lower porosity grow faster than those with many pores (Covey-Crump 1997; Olgaard and Evans 1988), and samples grow more slowly with increasing melt fraction (Renner et al. 2002).

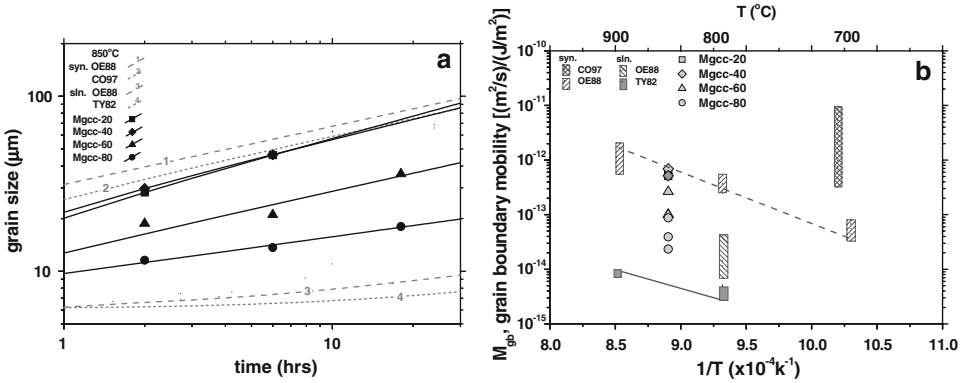

Fig. 9 **a** Grain growth data compiled for pure synthetic calcite from Olgaard and Evans 1988 (OE88, *line 1*), Covey-Crump 1997 (CO97, *line 2*); for Solnhofen limestone from Olgaard and Evans 1988, and Schmid 1977 (*line 3*), Tullis and Yund 1982 (TY82, *line 4*); and for synthetic Mg-calcite (*symbols with solid lines*; this study). Details of grain growth kinetics are compiled in Table 2. **b** Grain boundary mobility (m^2/s)/(J/m^2) as a function of inverse temperature (1/*T*) for different calcite rocks

Grain growth is often represented by an equation of the form:

$$d^p - d_0^p = k(t - t_o) \quad (4)$$

where k is a kinetic parameter, d and d_o are the average grain sizes at time, t and t_o, respectively. The exponent p is determined by the mechanisms operating during grain growth (Atkinson 1988; Brook 1976; Evans et al. 2001). Since our samples undergo a chemical reaction at the initial stage (Herwegh et al. 2003), we chose d_0 and t_0 to be 5 μm and 1,000 s (see above) and invert for p and k. Best-fit values for p vary from 2.4 to 4.7 for different Mg-calcites (Table 2). Such exponents are compatible with solute-drag ($p = 3$) (Evans et al. 2001; Yan et al. 1977) or pore-drag ($p = 2$–4) (Covey-Crump 1997; Spears and Evans 1982). Our HIPed samples have porosities of less than 1%; the porosity does not appear to correlate with Mg content. Some pore shapes do suggest boundary drag, however, so both solute-drag and pore-drag controlled mechanisms may be active in controlling the overall grain growth rate of Mg-calcite.

In agreement with earlier results (Herwegh et al. 2003), our data clearly indicate that grain-boundary mobility is inversely related to the Mg content (Fig. 9b). Here, we have calculated mobility using

$$M = \frac{1}{2} \times \frac{d}{\gamma} \times \frac{\partial d}{\partial t},$$

where grain-boundary energy, γ, is taken as 0.1 J/mol (Janczuk et al. 1983). Notice, however, that the addition of other solid solutes might have different effects on boundary mobility. For example, Freund et al. (2001) found the grain-growth rate of synthetic calcite made from powders ground from a single crystal containing elevated levels of Mn were faster than those made from crystals with less Mn. At present, the reason for this difference is not clear. Both Mn and Mg have ionic radii smaller than Ca, so the effect is not simply due to a change of sign of the misfit elastic

Table 2 Some laboratory determination of grain growth parameters in calcite aggregates

	T (°C)	*P* (MPa)	k ($\mu m^n/s$)	*n*	*Q* (kJ/mol)	t_0 (*s*), d_0 (μm)	Reference
Solnhofen	800	300	0.02–0.2	>7	190	0, 6.1	Schmid et al. (1977a)
	900	300	0.08–0.4	4.8	190		
	800	1,500	0.05–0.5	5.1	200	0, 6.1	Tullis and Yund
	900	1,500	0.8–1.0	3.0	200		(1982)
	800	300	0.03–0.13	5.2		0, 6.1	Olgaard and Evans (1988)
	900	300	0.1				
Syn. cc	800	300	2.4–2.8	2.6 ± 0.1	180 ± 50	0, 7	Olgaard and Evans (1988)
	706	185	0.15	2	232	1,000; 12	Covey-Crump (1997)
Mgcc-20	850	300	0.17	2.4		1,000; 5	This study
Mgcc-40	850	300	0.43	2.7		1,000; 5	This study
Mgcc-60	850	300	0.15	2.9		1,000; 5	This study
Mgcc-80	850	300	1.73	4.7		1,000; 5	This study

strain of the solute. Unlike Mg, Mn may be an aliovalent substitution and might thus affect the concentration of some point defect. Additionally, the bulk level of impurity in the two studies differs by an order of magnitude: i.e., <0.1 mol% Mn, versus up to 17 mol% Mg. Although our samples do not show chemical inhomogeneity at the level of electron microprobe observations, finer scale modulations of chemistry may be present in high Mg-calcite (Reeder 1983; Wenk et al. 1983). Tetard et al. (1999) found increased grain-growth rates in calcite doped with <1 wt% $LiPO_4$, but lower rates at higher concentrations (>2 wt%); they posited that solute was segregated into grain boundaries at high solute concentrations. However, it should be noted that lithium and calcium carbonates form a eutectic system at temperatures above 650°C, especially if the system contains water.

Using the elastic distortion model (Blundy and Wood 1994), we can estimate the amount of solute segregated into grain boundaries owing to elastic misfit of the solute to be about five times the concentration in the bulk material. The mobility predicted by such solute models (Blundy and Wood 1994; Blundy and Wood 2003; Hiraga et al. 2004) is

$$M = \frac{D_s \times \Omega}{2\delta kT(C_s e^{U/RT})},$$

where D_s is the lattice diffusion coefficient of the solute, Ω is the unit cell volume, δ is the grain boundary thickness, C_s is the concentration of solute at grain boundaries, and U is the energy associated with the partitioning of the solute into the grain boundary. In this case, boundary mobility should be reduced by about one order of magnitude when high Mg-calcite (17.0 mol%) is compared to low Mg-calcite (0.5 mol%). However, the mobility predicted by this relation is much slower than that determined from the grain growth data [$2 \times 10^{-16} - 3 \times 10^{-15}$ versus $2 \times 10^{-14} - 7 \times 10^{-13}$ $(m^2/s)/(J/m^2)$]. Other factors might also influence boundary mobility. For example, if pore drag is important in grain coarsening, then surface diffusion, rather than grain-boundary diffusion might limit growth. Thus, although it is clear that boundary mobility is adversely affected by additions in Mg solute, it is difficult to be definite about the exact cause of the reduction.

Composite flow law

The conditions of the experiments span a transition in mechanical behavior, which we interpret to involve a transition from diffusion creep to dislocation creep. In the transitional regime, both mechanisms may be active under a given set of loading conditions. To separate the effect of solutes on the individual mechanisms, we used a nonlinear generalized inversion method (Sotin and Poirier 1984) to fit the experimental data to Eq. (5); Eqs. (1) and (3) are used to describe diffusion and dislocation creep, respectively.

A number of different schemes can be used to compute the total strain rate of a material deforming by two mechanisms. For example, if there are two separate fractions within the aggregate, each of which are deforming exclusively by either diffusion or dislocation creep, the total strain rate can be estimated as the volume weighted sum (Ter Heege et al. 2004):

$$\dot{\varepsilon}_{tot} = v_{disl}\dot{\varepsilon}_{disl} + v_{diff}\dot{\varepsilon}_{diff} \quad (5)$$

where $\dot{\varepsilon}_{disl}$ is given either by Eq. (2) or Eq. (3), and $\dot{\varepsilon}_{diff}$ is given by Eq. (1); v_{disl} and v_{diff} are the volume fractions deforming by a particular mechanism. Alternatively, one might postulate that all grains are the same size and capable of deforming by both mechanisms, in which case $v_{disl} = v_{diff} = 1$ and the total deformation rate is simply the sum of the two creep laws. The estimate gained from this model is equivalent to a Sachs model where all grains in the aggregate are loaded under the same stress and can deform by either or both mechanisms.

In the following data inversions, we assume all grains are the average grain size and that all grains deform at rates set by Eqs. (1) and (3). In order to minimize the number of variables in the inversions, some other informed choices of the materials parameters had to be made. The activation energy for diffusion creep has been estimated as 200 ± 30 kJ/mol (Herwegh et al. 2003), and 210 kJ/mol for Solnhofen limestone (Schmid 1977). In these fits, we used a constant value of 212 kJ/mol for Q_{diff}, which we derive at a differential stress of ~20 MPa and temperatures of 700–800°C using equation $Q_{diff} = -R\partial \ln \dot{\varepsilon}/\partial(1/T)|_{\sigma}$. This value is higher than Hewrwegh at al.'s number but within the error limits, ±30 kJ. If we fix Q_{diff} to be 200 kJ/mol, the quality of fit changes only slightly.

The melting temperature T_m of calcite is reduced by the addition of Mg impurity (Byrnes and Wyllie 1981; Irving and Wyllie 1975). Variables in the dislocation creep law (3), which are essentially an empirical fit to many data sets, are not well known. We assumed that the grain size exponent m_p in the expression used for the Peierl stress in Eq. (3) is either 0.5 or 1. Fortunately, the results of the inversion vary only slightly when different values for m_p are used (Table 3). In general, within experimental uncertainties and sample-to-sample variations, the data can be fit well by the unconstrained inversion (Table 3 and Fig. 10). Figure 10 shows the best fits of the composite flow law to both Mg-calcite and synthetic calcite. The experimental data of Mn–calcite (Freund et al. 2004; Wang et al. 1996) are also plotted for comparison. Other constitutive laws for dislocation creep can also be used to fit the data, e.g., the power law [Eq. (2) and Table 3] or a stress activated law

Table 3 Fitting the data using hybrid flow law

	N	m_p	$\ln A_{plb}$ (MPa^{-2} s^{-1})	$\Sigma_{p,0}$ (MPa^{-1}kK^{-1})	lnk (MPa μm^m kK^{-1})	Q_{plb} (kJ mol^{-1})	$\aleph_\sigma$
Solnhofen	32	0.5	6.1 ± 0.5	19.9 ± 11.0	4.7 ± 0.2	205 ± 24	1.005 ± 0.102
		1[a]	5.9 ± 0.6	29.7 ± 9.5	5.1 ± 0.2	205 ± 14	1.005 ± 0.098
Syn. cc	82	1	4.3 ± 0.5	23.5 ± 1.5	2.8 ± 0.7	191 ± 24	1.015 ± 0.128
Mgcc-20	5	0.5	4.4 ± 1.1	8	5	201 ± 10	1.003 ± 0.107
		1	1.7 ± 1.2	8	5	201 ± 10	1.002 ± 0.021
Mgcc-40	5	0.5	3.5 ± 1.1	8	5	201 ± 10	1.001 ± 0.044
Mgcc-60	54	0.5	3.2 ± 0.6	41.2 ± 4.2	4.1 ± 0.2	201 ± 15	1.025 ± 0.160
			−3.3 ± 1.1	8	5	180 ± 10	1.043 ± 0.175
		1	−2.0 ± 0.7	30.7 ± 5.3	0.6 ± 4.3	197 ± 20	1.028 ± 0.152
Mgcc-70	42	0.5	−2.1 ± 1.3	35.5 ± 11.2	2.0 ± 0.9	196 ± 20	1.018 ± 0.157
		1	−1.2 ± 0.9	45.1 ± 6.3	0.7 ± 1.1	198 ± 22	1.007 ± 0.057
Mgcc-80	43	0.5	2.0 ± 0.6	12.0 ± 11.7	7.8 ± 0.3	181 ± 12	1.027 ± 0.213
			−4.6 ± 1.2	8	5	202 ± 10	0.984 ± 0.036
		1	2.1 ± 0.6	11.9 ± 11.7	9.3 ± 0.3	182 ± 15	1.026 ± 0.211

	N	$\ln\dot{\varepsilon}_{pwr0}$ (MPa^{-2} s^{-1})	n	Q_{pwr} (kJ mol^{-1})	$\aleph_\sigma$
Solnhofen	32	2.6 ± 0.6	3.4 ± 0.1	209 ± 4	1.014 ± 0.158
Syn. cc	82	−0.8 ± 0.5	4.3 ± 0.1	196 ± 16	1.017 ± 0.140
Mgcc-20	5	−0.7 ± 2.2	3.9 ± 0.6	201 ± 5	1.011 ± 0.097
Mgcc-40	5	−0.4 ± 1.9	3.6 ± 0.5	201 ± 5	1.009 ± 0.082
Mgcc-60	54	−12.5 ± 1.3	5.6 ± 0.3	202 ± 18	1.032 ± 0.154
Mgcc-70	42	−9.6 ± 1.7	5.0 ± 0.4	200 ± 20	1.018 ± 0.119
Mgcc-80	43	0.1 ± 0.8	2.6 ± 0.1	188 ± 15	1.015 ± 0.183

[a] We use 1,327 and 1,241°C as melting temperatures (T_m) for Mgcc-20 and Mgcc-80, respectively (Byrnes and Wyllie 1981; Irving and Wyllie 1975)

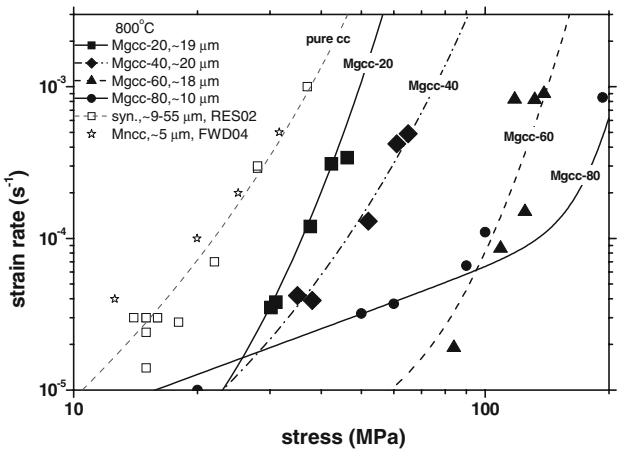

Fig. 10 Strength data and the curves fit using composite flow law (Eqs. (1), (3), and (5)). Parameters used see Table 3. The experimental data of Mn-calcite (Freund et al. 2004) and synthetic calcite (Renner et al. 2002) are also plotted for comparison

for cross slip. The relative effect of Mg concentration on the strength is similar for all the flow laws.

The apparent activation energies for dislocation creep from the inversion vary slightly for different Mg-calcites (~200 kJ/mol, see Table 3). Rather than inverting for the activation energies, they may also be calculated using $Q_{disl} = -R\partial \ln \dot{\varepsilon}/\partial(1/T)|_\sigma$. At a differential stress of ~90 MPa and temperatures of 700–800°C, the activation energies are 300 ± 74, 203 ± 64 and 145 ± 60 kJ/mol for Mgcc-60, Mgcc-70, and Mgcc-80, respectively; these values might be biased because grain sizes, and, therefore, strength evolve with different rates during the experiments. For example, the activation energy will be underestimated if it is determined from tests on samples where the initial grain size is systematically smaller at lower temperatures. Since dynamic recrystallization is prominent in Mgcc-80 (Fig. 3f) after deformation, its activation energy is likely to be underestimated using this method. Our derived values (Q_{plb}) are comparable to the activation energies for dislocation recovery kinetics of calcite single crystals (184 ± 22 kJ/mol, Liu and Evans 1997), and for dislocation creep of various calcite aggregates; e.g., about 200 kJ/mol for pure crystal aggregates (Renner et al. 2002), but are smaller than that for determined for dislocation creep of single crystals, 350 kJ/mol (de Bresser and Spiers 1993; Rutter 1974).

Effect of Mg on creep strength of high-magnesian calcite

Comparing our results with previous studies, we find that the strengths of synthetic aggregates (Renner et al. 2002), Solnhofen limestone (Schmid 1976, 1977), and Mg-calcite (this study) are nearly the same when grain sizes are less than 10 μm (Fig. 11). At a given strain rate and temperature, the strength varies inversely with the average grain size cubed, suggesting a Coble creep mechanism. For coarser-grained carbonates, dislocation creep dominates and the relation between grain size and strength is similar to a Hall–Petch relation. Increasing the magnesium content increases both the creep strength and the grain size at which the transition between the two deformation regimes occurs. In addition, we note that, in the high stress regime, both Yule marble (Heard 1963; Heard and Raleigh 1972) and Carrara marble (Covey-Crump 1997; de Bresser et al. 2001; Rutter 1995; Schmid et al. 1980) are stronger than the synthetic aggregates and single crystals.

To understand the strengthening behavior of calcite with Mg solute, we first notice that dolomite is much stronger than the high-magnesian calcite (Davis et al. 2003). There are several possible reasons for such strengthening, including larger elastic constants, solid-solution hardening, and precipitation hardening. The elastic modulus of calcite does increase with Mg concentration (Zhang and Reeder 1999), but only by ~16%, whereas, we observe increases in flow strength in the magnesian calcites of about 500% (Fig. 12). This solute hardening is very intriguing because of the possibility of complex interactions between solute cations and anions that might significantly alter the activity on different slip systems (Poirier, 1985). Solid solutes might affect the strength by affecting dislocation climb if the solutes affect point defect concentrations, or by decreasing dislocation mobility owing to impurity drag. It is also possible that the addition of magnesium solute introduces precipitates or sub-microscopic regions of cation order (Reeder 2000; Wenk et al. 1991), and that these structures act as impediments (discrete obstacles) to dislocation motion.

Solid-solute hardening, either by impurity drag or discrete obstacles, seems most probable. It is common for metal alloys and ceramics (Duong et al. 1993; Duong et al. 1994; Mohamed and Langdon 1975) to exhibit solute-hardening behavior during glide-controlled dislocation creep. Defects, including dislocations and grain boundaries, may generate solute atmospheres which retard dislocation glide (Cottrell and Jaswon 1949). The actual retarding force depends on the details of the concentration profiles, diffusivities, and activation energies, but in general, the strain rate is inversely proportional to the impurity concentration. At a fixed strain rate of 10^{-3} s^{-1} and 800°C, the strength of calcite monotonically increases with Mg concentration (Fig. 12) and is proportional to the cube root of the solute concentration C_{Mg}. However, if we predict the strength of the Mg-calcite using the solute-drag model of

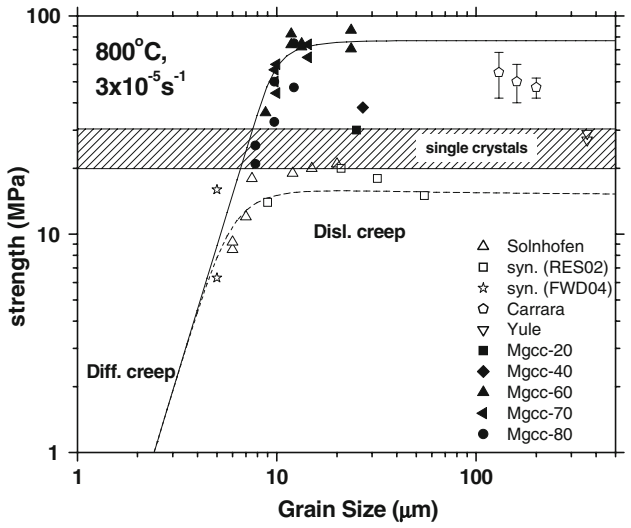

Fig. 11 Flow strength versus grain size for deformation of Mg-calcite (*solid symbols*) and previous studies on calcite aggregates (*open symbols*) at strain rate of 3×10^{-5} s^{-1}. When grain size is small, flow strength is approximately proportional to the grain size with grain size sensitivity factor ($m \approx 3$). References: Solnhofen limestone (Schmid 1976, 1977); synthetic marbles (syn., Renner et al. 2002 (RES02); Freund et al. 2004 (FWD04)); Carrara marble (Covey-Crump 1997 (147 μm); de Bresser 2002 (200 μm); Rutter 1995 (130 μm); Schmid et al. 1980 (150 μm)); Yule marble (Heard 1963; Heard and Raleigh 1972); and single crystals (de Bresser and Spiers 1993). The dashed line represents the best fit of the hybrid law to the data for Solnhofen limestone (Parameters see Table 3)

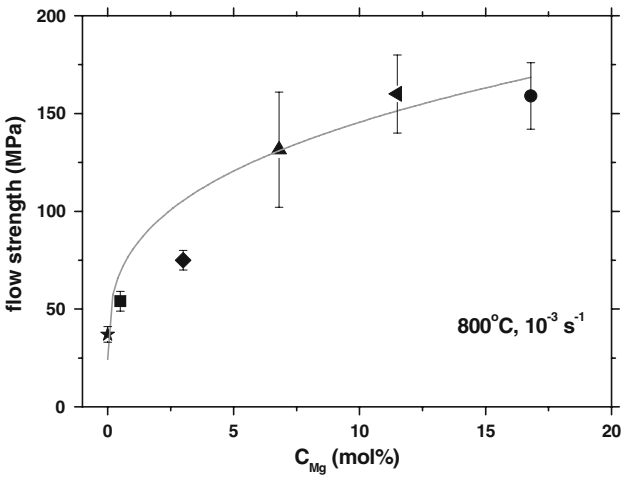

Fig. 12 Correlation between flow strength and Mg-content. At a temperature of 800°C and strain rate of 10^{-3} s^{-1}, the samples deform in dislocation creep regime. The flow strength of calcite increases with Mg concentration. *Dashed line* shows the flow strength as a function of the solute concentration (C_s) to the 1/3 power

Kitabjian et al. (1999), then the predicted strength is an order of magnitude greater than that observed. The obstacle mechanisms is also possible: natural high-magnesian calcite is known to exhibit nano-meter scale modulations in cation chemistry (Wenk et al. 1991), such modulations may be present in the synthetic samples, too.

In contrast to the results for Mg doping, a previous study (Freund et al. 2004) indicated that Mn solute seemed to decrease the diffusion creep strength. The reason for this difference between the two solutes is not clear, but Mn solute is multivalent and could affect charge neutrality conditions, and thus, the defect concentrations.

Natural applications

Natural carbonate rocks show variations in strength that may arise from differences in grain size, accessory minerals, porosity, or chemical impurities. These variations are of great concern when extrapolating flow laws into natural conditions or reconstructing paleo-deformation conditions from the interpretation of microstructures. For example, non-soluble, solid second phases can suppress grain growth by boundary pinning and change the overall strength of material (Evans et al. 2001; Knipe 1980; Olgaard and Evans 1988; Tullis and Yund 1982). If solid solution is possible, dissolved impurities could also affect grain-growth kinetics and creep behavior (Freund et al. 2001, 2004; Herwegh et al. 2003; Tetard et al. 1999). Mg is one, among several, possible cation solutes in calcite rocks, e.g., Mn, Fe, Sr; and these solutes may affect the creep behavior, as briefly demonstrated by de Bresser (1991). The experiments clearly indicate that Mg doping increases strength in the dislocation creep regime; and the transition from diffusion to dislocation creep at a fixed strain rate also occurs at a larger grain size as well. In at least some natural carbonates, the effects of magnesium content may be evident in the microstructure. We extrapolate the flow law of Mg-calcite to geological strain rates (10^{-12} s^{-1}) and compare this with pure calcite (Fig. 13). Naturally deformed carbonates also show evidence of chemical influences on strength. For example, Fig. 14 shows a porphyroblasts of high-magnesian calcite grains from echinoderm fossils that are much less deformed than surrounding carbonate matrix with lower Mg content. It seems clear that solute impurities will affect the strength of carbonates and that field interpretations will need to take this effect into account.

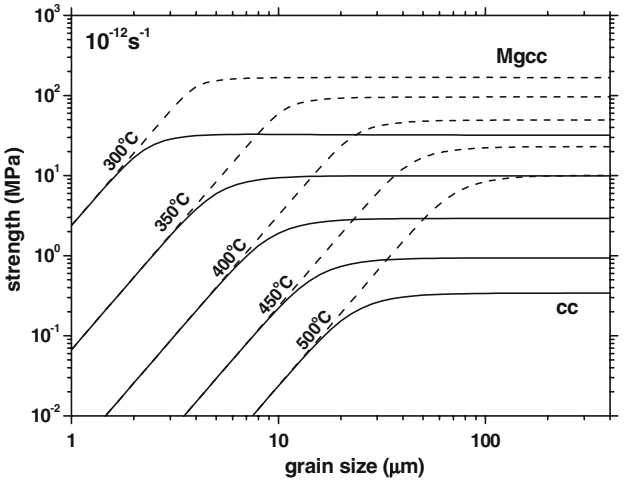

Fig. 13 Curves of stress versus grain size extrapolated to a strain rate of 10^{-12} s^{-1} at temperatures from 300 to 500°C. Mg-calcite and calcite are represented by the *dashed lines* and *solid lines*, respectively. High-magnesian calcite is much stronger compared with pure calcite in the dislocation creep regime; the transition from diffusion to dislocation moves to much higher stress

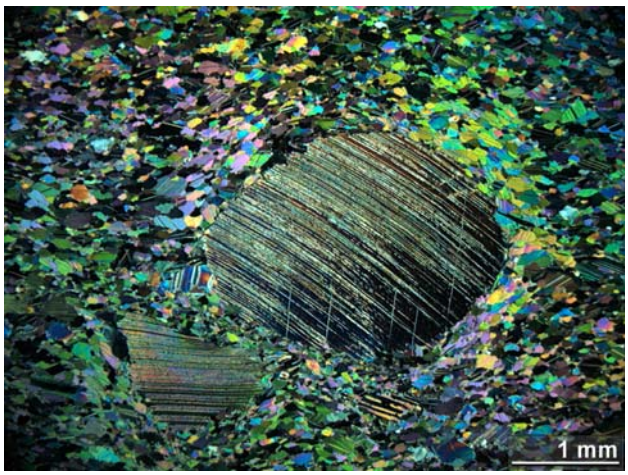

Fig. 14 Optical micrograph of carbonate mylonite from the Urgonian of the Morcles Nappe (Andreas), which contains echinoderms. These echinoderm fragments (*center* and *lower left*) consist of Mg-calcite and are stronger and thus less deformed than the surrounding fine-grained and completely recrystallized calcite matrix

Summary

Previous results (Herwegh et al. 2003) indicated that diffusion creep in high-magnesian calcite was not sensitive to the Mg content, but that grain growth was reduced by the addition of that solute. The results of this study corroborate those in the earlier work. Additional analyses indicate that the grain-growth rate of calcite is suppressed by >3.0 mol% Mg solute; and the grain growth exponent, p, ranges from 2.4 to 4.7 for different Mg-calcites. There are several mechanisms that might be active in controlling the overall grain growth rate, including solute-drag or pore-drag. No direct measurements of grain-boundary chemistry were made here, but solute segregation, if it occurs, is likely to reduce the grain-boundary mobility and would

explain the reduced grain growth rate. Nano-scale modulations in cation chemistry within the crystals might also be responsible. Reduction in grain size and suppression of grain-growth rate of Mg on calcite rocks might also be important for strain localization. Thus, variations in dolomite content within layered carbonate sediments might drastically affect calcite grain size during metamorphic process.

Although these experiments show that there is no obvious effect of Mg content on the strength of calcite in the diffusion creep regime ($\sigma < 40$ MPa) at temperature of 700–800°C, the transition between diffusion to dislocation creep regimes occurs at higher stresses for samples with higher Mg content and smaller grain size. In addition, the additional data collected here and the non-linear inversion of these data indicate that the Mg solute strengthens calcite in the dislocation creep regime, possibly as a result of local lattice distortions or owing to interactions between dislocations and solute ions/nanometer-scale domains of ordered cations. Our data suggest that, for a fixed temperature, strain rate, and grain size, the strength of calcite deforming by dislocation creep will depend on the cube root of the Mg concentration. Such chemical influences should be taken into account in field situations.

TEM observations indicate that dislocation recovery processes occur under the conditions of these experiments, and it is plausible that both dislocation climb and glide play important roles in controlling the overall strength of Mg-calcite in the dislocation creep regime.

Acknowledgments We acknowledge Xiaohui Xiao who provides us extensive assistance with the Paterson Rig at MIT. We benefited from the help from Ulrich Mok, Jock Hirst, Nilanjan Chatterjee, and Yong Zhang with our experimental studies. We are grateful for the constructive comments by the Editor, Jonathan Blundy, and anonymous reviewers, which have helped us to improve the manuscript. This research was supported by NSF's grant EAR-050412 and 0711139.

References

Anovitz LM, Essene EJ (1987) Phase-equilibria in the system caco3-mgco3-feco3. J Petrol 28(2):389–414

Atkinson HV (1988) Theories of normal grain-growth in pure single-phase systems. Acta Metall 36(3):469–491. doi:10.1016/0001-6160(88)90079-X

Bae SI, Baik S (1994) Critical concentration of mgo for the prevention of abnormal grain-growth in alumina. J Am Ceram Soc 77(10):2499–2504. doi:10.1111/j.1151-2916.1994.tb04634.x

Bai Q, Wang ZC, Kohlstedt DL (1995) Manganese olivine. 1. Electrical conductivity. Phys Chem Miner 22(8):489–503. doi:10.1007/BF00209374

Barnhoorn A, Bystricky M, Burlini L, Kunze K (2004) The role of recrystallisation on the deformation behavior of calcite rocks: Large strain torsion experiments on Carrara marble. J Struct Geol 26(5):885–903. doi:10.1016/j.jsg.2003.11.024

Bestmann M, Kunze K, Matthews A (2000) Evolution of a calcite marble shear zone complex on Thassos island, Greece: microstructural and textural fabrics and their kinematic significance. J Struct Geol 22(11–12):1789–1807. doi:10.1016/S0191-8141(00)00112-7

Blundy J, Wood B (1994) Prediction of crystal-melt partition-coefficients from elastic-moduli. Nature 372(6505):452–454. doi:10.1038/372452a0

Blundy J, Wood B (2003) Partitioning of trace elements between crystals and melts. Earth Planet Sci Lett 210(3–4):383–397

Brook RJ (1976) Controlled grain growth. In: Wang F-Y (ed) Ceramic fabrication procedures. Academic Press, New York

Bruhn DF, Olgaard DL, Dell'Angelo LN (1999) Evidence for enhanced deformation in two-phase rocks: experiments on the rheology of calcite-anhydrite aggregates. J Geophys Res Solid Earth 104(B1):707–724. doi:10.1029/98JB02847

Burkhard M (1990) Aspects of the large-scale Miocene deformation in the most external part of the Swiss Alps (sub-Alpine molasse to Jura fold belt). Eclogae Geol Helv 83(3):559–583

Burkhard M (1993) Calcite twins, their geometry, appearance and significance as stress–strain markers and indicators of tectonic regime—a review. J Struct Geol 15(3–5):351–368. doi:10.1016/0191-8141(93)90132-T

Busch JP, Vanderpluijm BA (1995) Calcite textures, microstructures and rheological properties of marble mylonites in the bancroft shear zone, Ontario, Canada. J Struct Geol 17(5):677–688. doi:10.1016/0191-8141(94)00092-E

Byrnes AP, Wyllie PJ (1981) Subsolidus and melting relations for the join caco3-mgco3 at 10-kbar. Geochim Cosmochim Acta 45(3):321–328. doi:10.1016/0016-7037(81)90242-8

Carter KE (1992) Evolution of stacked, ductile shear zones in carbonates from midcrustal levels—Tuscan nappe, n-apennines, Italy. J Struct Geol 14(2):181–192. doi:10.1016/0191-8141(92)90055-2

Chiang Y-M, Dunbar B, Kingery WD (1997) Physical ceramics: principles for ceramics science and.Engineering. Mit series in materials science and engineering. Wiley, New York, p 522

Chokshi AH, Yoshida H, Ikuhara Y, Sakuma T (2003) The influence of trace elements on grain boundary processes in yttria-stabilized tetragonal zirconia. Mater Lett 57(26–27):4196–4201. doi:10.1016/S0167-577X(03)00289-1

Cottrell AH, Jaswon MA (1949) Distribution of solute atoms round a slow dislocation. Proc R Soc Lond A Math Phys Sci 199:104–114. doi:10.1098/rspa.1949.0128

Covey-Crump SJ (1997) The normal grain growth behavior of nominally pure calcitic aggregates. Contrib Mineral Petrol 129(2–3):239–254. doi:10.1007/s004100050335

Covey-Crump SJ (1998) Evolution of mechanical state in Carrara marble during deformation at 400° to 700°C. J Geophys Res Solid Earth 103(B12):29781–29794. doi:10.1029/1998JB900005

Covey-Crump SJ (2001) Variation of the exponential and power law creep parameters with strain for Carrara marble deformed at 120 degrees to 400 degrees c. Geophys Res Lett 28(12):2301–2304. doi:10.1029/2000GL012692

Davis N, Kronenberg A, Newman J (2005) Plasticity and diffusion creep of dolomite. American Geophysical Union, Fall meeting 2005, abstract# MR33A-0152

Davis NE, Newman J, Kronenberg AK (2003) High temperature deformation of stoichiometric dolomite. AGU 2003:S22A–0433

de Bresser H, Evans B, Renner J (2002) Estimating the strength of calcite rocks under natural conditions. In: de Meer S, Drury MR, de Bresser JHP, Pennock G (eds) Deformation mechanisms, rheology, tectonics, current status future perspectives. Geolog. Society of London, London, pp 293–307

de Bresser JHP (1991) Intracrystalline deformation of calcite. Geol Ultraiectina 79:1–191

de Bresser JHP (1996) Steady state dislocation densities in experimentally deformed calcite materials: single crystals versus polycrystals. J Geophys Res Solid Earth 101(B10):22189–22201. doi:10.1029/96JB01759

de Bresser JHP (2002) On the mechanism of dislocation creep of calcite at high temperature: inferences from experimentally measured pressure sensitivity and strain rate sensitivity of flow stress. J Geophys Res Solid Earth 107(B12). doi:10.1029/2002JB001812

de Bresser JHP, Spiers CJ (1993) Slip systems in calcite single crystals deformed at 300–800°c. J Geophys Res Sol Earth 98(B4):6397–6409. doi:10.1029/92JB02044

de Bresser JHP, Ter Heege JH, Spiers CJ (2001) Grain size reduction by dynamic recrystallization: can it result in major theological weakening? Int J Earth Sci 90(1):28–45. doi:10.1007/s005310000149

de Bresser JHP, Urai JL, Olgaard DL (2005) Effect of water on the strength and microstructure of Carrara marble axially compressed at high temperature. J Struct Geol 27(2):265–281. doi:10.1016/j.jsg.2004.10.002

Dresen G, Evans B, Olgaard DL (1998) Effect of quartz inclusions on plastic flow in marble. Geophys Res Lett 25(8):1245–1248. doi:10.1029/98GL00730

Drury MR, Urai JL (1990) Deformation-related recrystallization processes. Tectonophysics 172(3–4):235–253. doi:10.1016/0040-1951(90)90033-5

Duong H, Beeman M, Wolfenstine J (1993) Creep-behavior of potassium-chloride rubidium chloride solid-solution alloys. J Am Ceram Soc 76(1):185–191. doi:10.1111/j.1151-2916.1993.tb03705.x

Duong H, Beeman M, Wolfenstine J (1994) High-temperature creep-behavior and substructure in kcl-kbr solid-solution alloys. Acta Metall Mater 42(3):1001–1012. doi:10.1016/0956-7151(94)90294-1

Essene EJ (1983) Solid solutions and solvi amoun metamorphic carbonates with applications to geologic thermobarometry. In: Reeder RJ (ed) Carbonates: mineralogy and chemistry. Reviews in mineralogy. American Mineralogical Society, Washington, DC, pp 77–96

Evans B, Renner J, Hirth G (2001) A few remarks on the kinetics of static grain growth in rocks. Int J Earth Sci 90(1):88–103. doi:10.1007/s005310000150

Freund D, Rybacki E, Dresen G (2001) Effect of impurities on grain growth in synthetic calcite aggregates. Phys Chem Miner 28(10):737–745. doi:10.1007/s002690100196

Freund D, Wang ZC, Rybacki E, Dresen G (2004) High-temperature creep of synthetic calcite aggregates: influence of Mn-content. Earth Planet Sci Lett 226(3–4):433–448. doi:10.1016/j.epsl.2004.06.020

Frost HJ (1982) Deformation mechanism and fracture mechanism maps. CIM Bull 75(842):110–110

Goetze C, Kohlstedt DL (1977) Dislocation-structure of experimentally deformed marble. Contrib Mineral Petrol 59(3):293–306. doi:10.1007/BF00374558

Griggs D, Miller WB (1951) Deformation of Yule marble: part I—compression and extension experiments on dry Yule marble at 10,000 atmospheres confining pressure, room temperature. Geol Soc Am Bull 62(8):853–862. doi:10.1130/0016-7606(1951)62[853:DOYMPI]2.0.CO;2

Heard HC (1960) Transition from brittle to ductile flow in Solnhofen limestone as a function of temperature, confining pressure, and interstitial fluid pressure rock deformation: Geological Society of America Memoir, 79:193–226

Heard HC (1963) Effect of large changes in strain rate in the experimental deformation of Yule marble. J Geol 71:162–195

Heard HC, Raleigh CB (1972) Steady-state flow in marble at 500° to 800°C. Geol Soc Am Bull 83(4):936–956. doi:10.1130/0016-7606(1972)83[935:SFIMAT]2.0.CO;2

Heitzmann P (1987) Calcite mylonites in the central Alpine root zone. Tectonophysics 135(1–3):207–215. doi:10.1016/0040-1951(87)90162-4

Herwegh M, Kunze K (2002) The influence of nano-scale second-phase particles on deformation of fine grained calcite mylonites. J Struct Geol 24(9):1463–1478. doi:10.1016/S0191-8141(01)00144-4

Herwegh M, Xiao XH, Evans B (2003) The effect of dissolved magnesium on diffusion creep in calcite. Earth Planet Sci Lett 212(3–4):457–470. doi:10.1016/S0012-821X(03)00284-X

Hiraga T, Anderson IM, Kohlstedt DL (2004) Grain boundaries as reservoirs of incompatible elements in the earth's mantle. Nature 427(6976):699–703. doi:10.1038/nature02259

Hiraga T, Hirschmann MM, Kohlstedt DL (2007) Equilibrium interface segregation in the diopside-forsterite system ii: Applications of interface enrichment to mantle geochemistry. Geochim Cosmochim Acta 71(5):1281–1289. doi:10.1016/j.gca.2006.11.020

Hitchings RS, Paterson MS, Bitmead J (1989) Effects of iron and magnetite additions in olivine pyroxene rheology. Phys Earth Planet Inter 55(3–4):277–291. doi:10.1016/0031-9201(89)90076-9

Hobbs BE (1984) Point defect chemistry of minerals under a hydrothermal environment. J Geophys Res 89(B6):4026–4038. doi:10.1029/JB089iB06p04026

Irving AJ, Wyllie PJ (1975) Subsolidus and melting relationships for calcite, magnesite and join caco3-mgco3 to 36 kb. Geochim Cosmochim Acta 39(1):35–53. doi:10.1016/0016-7037(75)90183-0

Janczuk B, Chibowski E, Staszczuk P (1983) Determination of surface free-energy components of marble. J Colloid Interface Sci 96(1):1–6. doi:10.1016/0021-9797(83)90002-4

Jordan PG (1987) The deformational behavior of bimineralic limestone-halite aggregates. Tectonophysics 135(1–3):185–197. doi:10.1016/0040-1951(87)90160-0

Kitabjian PH, Garg A, Noebe RD, Nix WD (1999) High-temperature deformation behavior of NiAl(Ti) solid-solution single crystals. Metal Mater Trans Part A Phys Metal Mater Sci 30(3):587–600

Knipe RJ (1980) Distribution of impurities in deformed quartz and its implications for deformation studies. Tectonophysics 64(1–2):T11–T18. doi:10.1016/0040-1951(80)90255-3

Kohlstedt DL (2006) The role of water in high-temperature rock deformation, Water in nominally anhydrous minerals. Rev Mineral Geochem 62:377–396. doi:10.2138/rmg.2006.62.16

Kohlstedt DL, Evans B, Mackwell SJ (1995) Strength of the lithosphere—constraints imposed by laboratory experiments. J Geophys Res Solid Earth 100(B9):17587–17602. doi:10.1029/95JB01460

Liu M, Evans B (1997) Dislocation recovery kinetics in single-crystal calcite. J Geophys Res Solid Earth 102(B11):24801–24809. doi:10.1029/97JB01892

Lücke K, Stüwe HP (1971) On the theory of impurity controlled grain boundary motion. Acta Metall 19:1087–1099. doi:10.1016/0001-6160(71)90041-1

Mackenzie FT, Bischoff WD, Bishop FC, Loijens M, Schoonmaker J, Wollast R (1983) Magnesian calcites: Low-temperature occurrence, solubility, and solid-solution behavior. In: Reeder R (ed) Carbonates: Mineralogy and chemistry. Reviews in mineralogy. Mineralogical Society of America, Washington DC, pp 97–144

Mohamed FA, Langdon TG (1975) Creep-behavior of ceramic solid-solution alloys. J Am Ceram Soc 58(11–1):533–534

Molli G, Conti P, Giorgetti G, Meccheri M, Oesterling N (2000) Microfabric study on the deformational and thermal history of the Alpi apuane marbles (Carrara marbles), Italy. J Struct Geol 22(11–12):1809–1825. doi:10.1016/S0191-8141(00)00086-9

Molli G, Heilbronner R (1999) Microstructures associated with static and dynamic recrystallization of Carrara marble (Alpi apuane, nw tuscany, Italy). Geologie En Mijnbouw Neth J Geosci 78(1):119–126. doi:10.1023/A:1003826904858

Nesse WD (2000) Introduction to mineralogy. Oxford University Press, New York, p 442

Olgaard DL, Evans B (1986) Effect of 2nd-phase particles on grain-growth in calcite. J Am Ceram Soc 69(11):C272–C277. doi:10.1111/j.1151-2916.1986.tb07374.x

Olgaard DL, Evans B (1988) Grain-growth in synthetic marbles with added mica and water. Contrib Mineral Petrol 100(2):246–260. doi:10.1007/BF00373591

Paterson MS (1976) Some current aspects of experimental rock deformation. Philos Trans R Soc Lond Ser Part A Math Phys Eng Sci 283(1312):163–172

Paterson MS (1990) Rock deformation experimentation. Geophys Monogr 56:187–194

Paterson MS (2001) Relating experimental and geological theology. Int J Earth Sci 90(1):157–167. doi:10.1007/s005310000158

Pfiffner OA (1982) Deformation mechanisms and flow regimes in limestones from the helvetic zone of the Swiss Alps. J Struct Geol 4(4):429–442. doi:10.1016/0191-8141(82)90034-7

Pieri M, Burlini L, Kunze K, Stretton I, Olgaard DL (2001) Rheological and microstructural evolution of Carrara marble with high shear strain: results from high temperature torsion experiments. J Struct Geol 23(9):1393–1413. doi:10.1016/S0191-8141(01)00006-2

Poirier JP (1985) Creep of crystals; high-temperature deformation processes in metals, ceramics and minerals

Powers JD, Glaeser AM (1998) Grain boundary migration in ceramics. Interf Sci 6(1–2):23–39. doi:10.1023/A:1008656302007

Ranalli G, Murphy DC (1987) Rheological stratification of the lithosphere. Tectonophysics 132(4):281–295. doi:10.1016/0040-1951(87)90348-9

Reeder RJ (1983) Tem as a tool in study of carbonate crystal-chemistry. Aapg Bull Am Assoc Petrol Geol 67(3):538–539

Reeder RJ (2000) Constraints on cation order in calcium-rich sedimentary dolomite. Aquat Geochem 6(2):213–226. doi:10.1023/A:1009659122772

Renner J, Evans B (2002) Do calcite rocks obey the power-law creep equation? In: de Meer S, Drury MR, de Bresser JHP, Pennock GM (eds) Deformation mechanisms, rheology and tectonics: current status and future perspectives. Special publications. Geological Society, London, pp 293–307

Renner J, Evans B, Siddiqi G (2002) Dislocation creep of calcite. J Geophys Res Solid Earth 107(B12). doi:10.1029/2001JB001680

Renner J, Siddiqi G, Evans B (2007) Plastic flow of two-phase marbles. J Geophys Res Solid Earth 112(B7). doi:10.1029/2005JB004134

Rollett AD (2004) Modeling the impact of grain boundary properties on microstructural evolution. Recrystallization and grain growth, pts 1 and 2. Materials science forum, pp 707–714

Rutter EH (1972) The influence of interstitial water on the rheological behavior of calcite rocks. Tectonophysics 14(1):13–33. doi:10.1016/0040-1951(72)90003-0

Rutter EH (1974) Influence of temperature, strain rate and interstitial water in experimental deformation of calcite rocks. Tectonophysics 22(3–4):311–334. doi:10.1016/0040-1951(74)90089-4

Rutter EH (1984) The influence of temperature, strain rate, and interstitial water in the experimental deformation of calcite rocks. Tectonophysics 43:311–334

Rutter EH (1995) Experimental study of the influence of stress, temperature, and strain on the dynamic recrystallization of Carrara marble. J Geophys Res Solid Earth 100(B12):24651–24663. doi:10.1029/95JB02500

Rutter EH (1999) On the relationship between the formation of shear zones and the form of the flow law for rocks undergoing dynamic recrystallization. Tectonophysics 303(1–4):147–158. doi:10.1016/S0040-1951(98)00261-3

Rybacki E, Paterson MS, Wirth R, Dresen G (2003) Rheology of calcite-quartz aggregates deformed to large strain in torsion. J Geophys Res Solid Earth 108(B2):2089. doi:10.1029/2002JB001833

Schenk O, Urai JL, Evans B (2005) The effect of water on recrystallization behavior and grain boundary morphology in calcite-observations of natural marble mylonites. J Struct Geol 27(10):1856–1872. doi:10.1016/j.jsg.2005.05.015

Schmid SM (1976) Rheological evidence for changes in the deformation mechanism of solenhofen limestone towards low stresses. Tectonophysics 31(1–2):T21–T28. doi:10.1016/0040-1951(76)90160-8

Schmid SM (1977) Superplastic flow in fine-grained limestone. Tectonophysics 43(3–4):257–291. doi:10.1016/0040-1951(77)90120-2

Schmid SM, Paterson MS, Boland JN (1980) High temperature flow and dynamic recrystallization in Carrara marble. Tectonophysics 65(3–4):245–280. doi:10.1016/0040-1951(80)90077-3

Siddiqi G, Evans B, Dresen G, Freund D (1997) Effect of semibrittle deformation on transport properties of calcite rocks. J Geophys Res Solid Earth 102(B7):14765–14778. doi:10.1029/97JB01038

Sotin C, Poirier JP (1984) Ananlysis of high-temperature creep experiments by generalized nonlinear inversion. Mech Mater 3(4):311–317. doi:10.1016/0167-6636(84)90031-0

Spears MA, Evans AG (1982) Microstructure development during final intermediate stage sintering. 2. Grain and pore coarsening. Acta Metall 30(7):1281–1289. doi:10.1016/0001-6160(82)90146-8

Spiers CJ (1979) Fabric development in calcite polycrystals deformed at 400-degrees-c. Bull De Mineralogie 102(2–3):282–289

Ter Heege JH, de Bresser JHP, Spiers CJ (2004) Composite flow laws for crystalline materials with log-normally distributed grain size: Theory and application to olivine. J Struct Geol 26(9):1693–1705. doi:10.1016/j.jsg.2004.01.008

Tetard F, Bernache-Assollant D, Champion E (1999) Pre-eutectic densification of calcium carbonate doped with lithium carbonate. J Therm Anal Calorim 56(3):1461–1473. doi:10.1023/A:1010191414628

Tullis J, Yund RA (1982) Grain growth kinetics of quartz and calcite aggregates. J Geol 90(3):301–318

Urai JL, Means WD, Lister GS (1986) Dynamic recrystallization of minerals. In: Hobbs BEH and Hugh C (Eds) Mineral rock deformation: Laboratory studies, paterson volume. Geophysical Monograph, Washington DC, pp 161–200

Vanderpluijm BA (1991) Marble mylonites in the bancroft shear zone, Ontario, Canada - microstructures and deformation mechanisms. J Struct Geol 13(10):1125–1135. doi:10.1016/0191-8141(91)90073-R

Walker AN, Rutter EH, Brodie KH (1990) Experimental study of grain-size sensitive flow of synthetic, hot-pressed calcite rocks. In: Knipe RJ, Rutter EH (eds) Deformation mechanisms, rheology and tectonics. Geological Society Special Publications, pp 259–284

Wang ZC, Bai Q, Dresen G, Wirth R (1996) High-temperature deformation of calcite single crystals. J Geophys Res Solid Earth 101(B9):20377–20390. doi:10.1029/96JB01186

Wenk HR, Barber D, Reeder R (1983) Microstructures in carbonates. In: Reeder R (ed) Carbonates: Mineralogy and chemistry.

Reviews in mineralogy. American Mineralogical Society, Washington DC, pp 301–369

Wenk HR, Bulakh A (2004) Minerals, their constitution and origin. University Press, Cambridge, p 646

Wenk HR, Hu MS, Lindsey T, Morris JW (1991) Superstructures in ankerite and calcite. Phys Chem Miner 17(6):527–539. doi:10.1007/BF00202231

Xiao XH, Evans B (2003) Shear-enhanced compaction during nonlinear viscous creep of porous calcite-quartz aggregates. Earth Planet Sci Lett 216(4):725–740. doi:10.1016/S0012-821X(03)00536-3

Yan MF, Cannon RF, Bowen HK (1977) Grain boundary migration in ceramics. In: Fulrath RM, Pask JA (eds) Ceram microstructures—76. Westview Press, Boulder, pp 276–307

Yin XL (1996) The deformation mechanism of marble mylonites in the dashankou shear zone. J Geom 2(4):61–67

Zhang JZ, Reeder RJ (1999) Comparative compressibilities of calcite-structure carbonates: Deviations from empirical relations. Am Mineral 84(5–6):861–870

Zhao YH, Zimmerman M and Kohlstedt DL, in press (2008) Effect of iron content on the creep behavior of olivine: 1. Anhydrous conditions

Zhu WL, Evans B, Bernabe Y (1999) Densification and permeability reduction in hot-pressed calcite: a kinetic model. J Geophys Res Solid Earth 104(11):25501–25511. doi:10.1029/1999JB900230